Mechanics Research Communications 131 (2023) 104131

Contents lists available at ScienceDirect

Mechanics Research Communications

journal homepage: www.elsevier.com/locate/mechrescom

Mechanics and transient morphing of soft hygroscopic bilayers

Eman H.O. Alameen [a,*], Alessandro Lucantonio [a,b], Antonio DeSimone [a,c]

[a] The BioRobotics Institute, V.le R. Piaggio 34, Pontedera (PI), 56026, Italy
[b] Department of Mechanical and Production Engineering, Aarhus University, Inge Lehmanns Gade 10, Aarhus, 8000, Denmark
[c] SISSA, Via Bonomea 265, Trieste, 34136, Italy

ARTICLE INFO

Keywords:
Anisotropic hygroscopic material
Bilayer structure
Finite element method
Diffusion
Target metric

ABSTRACT

Motivated by pine cones and plant seeds that open or close in response to changes in humidity thanks to the shrinking or swelling of hygroscopic bilayers, and given the recent interest in artificial systems that mimic the hygroscopic motility of seeds, we consider bilayers consisting of two adhering elongated thin layers made of hygroscopic gels, modeled as active, transversally isotropic elastic materials. The direction of transverse isotropy is set as one of the fibers that are present in both biological and synthetic materials. As a special, biologically relevant case, we consider one of the two layers passive. This work develops a three-dimensional model for the coupled evolution of elastic deformations and moisture content (solvent concentration). Based on this model, a numerical scheme for solving the evolution equations coupling mechanical equilibrium and diffusion has been constructed based on the Finite Element Method. The equations are formulated in weak form and solved using Comsol Multiphysics. We have applied our model to compute transient configurations and their steady-state equilibrium limits in some relevant test cases. These configurations are then analyzed to understand the influence of the various geometric and physical parameters.

1. Introduction

Plants are stationary organisms that have developed fascinating strategies for seed dispersal during their natural evolution. Examples include reliance on transport by wind (thanks to the helical motion of the samaras of acers [1] or to the pappus of dandelions [2] that work as parachutes that slow down their vertical fall, giving them more time to cover lateral distances under the action of lateral winds) or transport by animals (to which seeds attach thanks to spiny spores).

The release mechanisms of plant seeds from pine cones [3] or seed pods in *Bauhinia variegata* [4] or *Cardamine hirsuta* [5] rely on the opening deformations induced by drying of hygroscopic bilayers. The same mechanism allows the awns of *Erodium cicutarium* to anchor firmly in the ground [6,7].

Besides their biological interest, seed dispersal strategies are inspiring a new concept for distributed environmental monitoring based on an ecosystem of plant seed-like soft robots [8,9]. Here we focus on the mechanics of morphing of natural seeds and of their engineered bio-inspired counterparts exploiting hygroscopic shrinking or swelling of a hygroscopic gel in a bilayer architecture.

Timoshenko pioneered the study of the bending mechanism of bilayers, highlighting that the temperature-induced bending of bimetallic strips results from the differences in thermal expansion coefficient in each layer [10]. The same concept is at play in hygroscopic bilayers, gel bilayers in particular, with humidity being the driving stimulus instead of temperature.

The dynamics of each active layer are controlled by the free-energy reduction caused by solvent absorption from the environment. This is driven by the competition between the entropy of mixing (which favors solvent absorption) and the free-energy cost of the elastic deformations required to accommodate volume changes caused by solvent absorption. Solvent diffusion within the hygroscopic materials governs the kinetics of this process. The creation of spontaneous curvature in response to changes in the humidity of the environment is driven by the continuity of displacements across the interface of the two heterogeneous layers.

The morphing behavior of hygroscopic bilayer structures has attracted considerable attention in recent literature, and several modeling approaches have been proposed. Change in the shape of pinecone-like and seedpod-like sheets, which correspond to systems with bending and twisting deformation modes, has been modeled using the concept of target metric and curvature tensors. The use of this concept has been pioneered in [11] and then applied to many material systems including, e.g., patterned gels [12], patterned films of liquid crystal elastomers [13], and many more.

In the context of plant seeds, Armon et al. pioneered the use of this approach, in which morphing thin films are treated as two-dimensional

* Corresponding author.
E-mail addresses: eman.hishamomeralameen@santannapisa.it (E.H.O. Alameen), desimone@sissa.it (A. DeSimone).

https://doi.org/10.1016/j.mechrescom.2023.104131
Received 30 January 2023; Received in revised form 26 April 2023; Accepted 17 May 2023
Available online 20 May 2023

surfaces with time-dependent target metric and curvature tensors, and studied in this way the seed pod opening in *Bauhinia variegata* [4]. Moreover, Abdelmohsen et al. created a 3D multiphysics numerical model to characterize the hygroscopic behavior of wood based on the non-linear theory of hyper-elastic solids. They considered the material's orthotropic elastic response and swelling behavior, assuming different swelling stretches in different directions [14]. Both these studies focus on equilibrium shapes and do not explicitly resolve solvent diffusion and transient shapes.

Coupled fluid diffusion and finite deformation have been studied in the context of swelling hydrogels. Nardinocchi et al. used the Flory–Rehner model to study thin bilayer hydrogel sheets with different anisotropic structures [15]. Liu et al. simulate the inhomogeneous anisotropic swelling in fiber-reinforced hydrogels. They added anisotropic effects into the model by including terms in the free energy depending on invariants related to fiber deformations [16]. They consider the elastic contribution of the deformation to the free energy but neglect the mixing contribution.

In this work, we developed a model for steady state and transient states (coupling diffusion/swelling and elasticity) in anisotropic hygroscopic bilayers utilizing (3D) non-linear elasticity. The model is able to predict transient and equilibrium configurations of hygroscopic bilayers similar to those observed in nature by *Erodium cicutarium*, whose awns are straight when dry and recoil to a helical shape when wet.

2. Free-energy density

We describe the behavior of an anisotropic hygroscopic bilayer under deformation and solvent diffusion, utilizing the Flory–Rehner model. This model's main unknowns (state variables) are two fields defined on the reference configuration $\mathcal{B}$, a subset of the three-dimensional ambient space. The first one is the point-valued deformation map f that gives the current position x of a point $X \in \mathcal{B}$ and the current configuration $f(\mathcal{B}_\tau)$ of the body. We denote by $F = \nabla f$ the deformation gradient and by $J = \det F$ the jacobian determinant. The second is the scalar field μ, representing the chemical potential.

Following the Flory–Rehner model for hydrogels [17,18], we write the free-energy density per unit reference volume as

$$W(C,\mu) = W_{el}(C) + W_{mix}\left((\det C)^{1/2}\right) - \frac{\mu}{\Omega}(\det C)^{1/2} \tag{2.1}$$

where $C = F^T F$ is the right Cauchy–Green strain tensor obtained from the deformation gradient $F = \nabla f$, W_{mix} is the solid-solvent free-energy of mixing defined below, and Ω is the solvent molar volume.

We assume that the elastic density energy $W_{el}(C)$ is the sum of the isotropic neo-Hookean term and a transversely isotropic correction inspired by [15,19].

$$W_{el}(C) = \frac{1}{J_0}\left(\frac{G}{2}\left[F_0^T C F_0 \cdot I - 3\right] + \gamma\frac{G}{2}\left[F_0^T C F_0 \cdot a \otimes a - 1\right]^2\right) \tag{2.2}$$

where I is the identity, a is the fiber orientation, $J_0 = \det F_0 = (\det C_0)^{\frac{1}{2}}$, G is the shear modulus, and γ is a modulus quantifying the degree of anisotropy. The tensor product $a \otimes b$ of vectors a and b is given in components by $(a \otimes b)_{ij} = a_i b_j$. In a bilayer geometry, these parameters may be different in the two layers. The first square bracket in Eq. (2.2) is the classical neo-Hookean term $\mathrm{tr}\left((FF_0)^T(FF_0) - 1\right)$. The second square bracket is the standard stiffing term based on the $I_4 = \left|FF_0 a\right|^2$. In both terms, the deformation is measured with respect to the dry state.

The concept of anisotropic materials can be modeled by adding energetic contributions based on certain deformation invariants, as in the second summand equation (2.2), which was introduced in the early 90s, and aimed to describe the effects of elastic anisotropic response [20,21]. To justify the choice for the terms in Eq. (2.2), we emphasize that, in this paper, we are not trying to model specific material systems in qualitative detail. The neo-Hookean energy and the one-invariant anisotropic correction in Eq. (2.2) are chosen only because they are the simplest possible expressions in the literature. Many other choices are possible [22], and selecting different terms in Eq. (2.2) may become necessary to match quantitatively properties like the stress–strain response of a specific artificial or biological material.

The choice of a reference configuration different from the dry one is a consequence of our choice of describing the solid–water mixing energy $W_{mix}(C)$, with the Flory–Huggins form, which is widely used to model the mixing behavior of the polymer network and the water molecules [23]. To avoid a singularity in this term for the dry state, we follow [24] and define a reference state slightly swollen compared to the dry one $\mathcal{B}_d$. We refer to this state as the free swollen state $\mathcal{B}$. The mixing energy is expressed by:

$$W_{mix}(J) = \frac{1}{J_0}\frac{RT}{\Omega}\left[\left(JJ_0 - 1\right)\log\left(\frac{JJ_0 - 1}{JJ_0}\right) + \chi\frac{JJ_0 - 1}{JJ_0}\right] \tag{2.3}$$

where R is the universal gas constant, T is the temperature, χ is Flory–Huggins interaction parameter, and $J = \det F = (\det C)^{\frac{1}{2}}$ is the jacobian determinant.

The swelling deformation from the dry to the reference state is described by F_0. We introduce the strain tensor $C_0 = F_0^T F_0$, and the swelling stretches in the direction parallel and perpendicular to the fiber $\lambda_{0\|}$, and $\lambda_{0\perp}$. In view of transversal isotropic symmetry, we can write

$$C_0 = \lambda_{0\|}^2 a \otimes a + \lambda_{0\perp}^2(\mathrm{I} - a \otimes a) \tag{2.4}$$

Using Eq. (2.4) and $\det C_0 = J_0^2$, we can write Eq. (2.3) in more explicit form

$$\begin{aligned} W_{mix}\left((\det C)^{\frac{1}{2}}\right) = \frac{RT}{\Omega}\Bigg[&\left(\frac{\lambda_{0\|}\lambda_{0\perp}^2(\det C)^{\frac{1}{2}} - 1}{\lambda_{0\|}\lambda_{0\perp}^2}\right) \\ &\log\left(\frac{\lambda_{0\|}\lambda_{0\perp}^2(\det C)^{\frac{1}{2}} - 1}{\lambda_{0\|}\lambda_{0\perp}^2(\det C)^{\frac{1}{2}}}\right) + \frac{\chi}{\lambda_{0\|}\lambda_{0\perp}^2}\frac{\lambda_{0\|}\lambda_{0\perp}^2(\det C)^{\frac{1}{2}} - 1}{\lambda_{0\|}\lambda_{0\perp}^2(\det C)^{\frac{1}{2}}}\Bigg] \end{aligned} \tag{2.5}$$

To simplify the highly nonlinear governing equations following from (2.1), we approximate the energy in (2.1) with a suitable harmonic expansion. In fact, for each value of the chemical potential μ, there is a preferred state (target state $\bar{C}(\mu)$) that minimizes energy (2.1) with respect to C at fixed μ. We consider a Taylor expansion at order 2 for the free energy $W(C,\mu)$ around $\bar{C}(\mu)$. The expression of the energy can then be written as

$$W(C,\mu) = W(C,\mu)|_{C=\bar{C}(\mu)} + \frac{1}{2}\left\langle \frac{\partial^2 W}{\partial C^2}\bigg|_{C=\bar{C}(\mu)}(C-\bar{C}),(C-\bar{C})\right\rangle \tag{2.6}$$

where the linear term is missing because $\frac{\partial W}{\partial C}\big|_{C=\bar{C}(\mu)} = 0$ by energy minimality, and $\langle .,. \rangle$ denotes the inner product of the vectors $(C - \bar{C})$.

3. Characterization of the reference state and the target state

The sketch in Fig. 1 my help the reader to grasp the overall structure of our model.

3.1. Reference state

The reference state, which is defined by $C = I = \bar{C}(\mu_0)$, is characterized by

$$\frac{\partial W}{\partial C}(C,\mu_0)\bigg|_{C=I=\bar{C}(\mu_0)} = 0 \tag{3.1}$$

This condition expresses the fact that the material is in equilibrium with zero stress when the external chemical potential is the one of the reference configuration $\mu_{ext} = \mu_0$.

In view of Eq. (2.4), the expression in Eq. (3.1) depends only on μ_0, $\lambda_{0\|}$ and $\lambda_{0\perp}$. As shown in Appendix A, imposing that Eq. (3.1) holds is

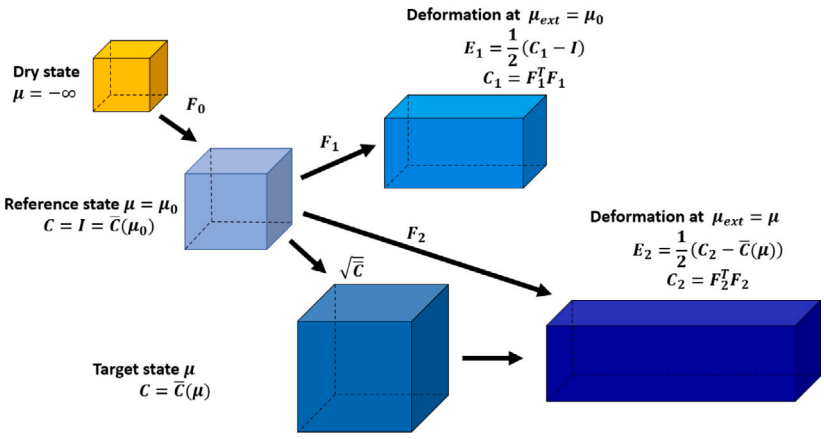

Fig. 1. Sketch of the dry, reference, and target configurations.

equivalent to imposing the following relations between $\lambda_{0\|}$, $\lambda_{0\perp}$, and μ_0:

$$\lambda_{0\perp}^2 = \lambda_{0\|}^2 \left(1 + 2\gamma \left(\lambda_{0\|}^2 - 1\right)\right) \tag{3.2}$$

$$\mu_0 = \frac{G\Omega}{\lambda_{0\|}} + RT \left[\log\left(\frac{\lambda_{0\|}\lambda_{0\perp}^2 - 1}{\lambda_{0\|}\lambda_{0\perp}^2}\right) + \frac{1}{\lambda_{0\|}\lambda_{0\perp}^2} + \frac{\chi}{{\lambda_{0\|}}^2\lambda_{0\perp}^4}\right] \tag{3.3}$$

These equations define $\lambda_{0\|}$ and $\lambda_{0\perp}$ implicitly as functions of μ_0 and will appear as constraints in the numerical implementation of our model (see Section 6).

3.2. Target state

The target state $\bar{C} = \bar{C}(\mu)$ corresponding to the value μ of the chemical potential is defined by the condition following from energy minimality

$$\frac{\partial W}{\partial C}(C, \mu)\Big|_{C=\bar{C}(\mu)} = 0 \tag{3.4}$$

where transversal isotropic symmetry implies that

$$\bar{C} = \bar{C}(\mu) = \bar{\lambda}_{\|}^2 a \otimes a + \bar{\lambda}_{\perp}^2 (I - a \otimes a) \tag{3.5}$$

As before, the expression in Eq. (3.4) depends only on μ, $\bar{\lambda}_{\|}$ and $\bar{\lambda}_{\perp}$. As shown in Appendix A, imposing that Eq. (3.4) holds is equivalent to imposing the following relations between $\bar{\lambda}_{\|}$, $\bar{\lambda}_{\perp}$, and μ :

$$\bar{\lambda}_{\perp}^2 = \frac{\lambda_{0\|}^2 \bar{\lambda}_{\|}^2}{\lambda_{0\perp}^2}\left[1 + 2\gamma\left(\lambda_{0\|}^2 \bar{\lambda}_{\|}^2 - 1\right)\right] \tag{3.6}$$

$$\mu = \frac{G\Omega}{\bar{\lambda}_{\|}\lambda_{0\|}} + RT\left[\log\left(\frac{\bar{\lambda}_{\|}\lambda_{0\|}\bar{\lambda}_{\perp}^2\lambda_{0\perp}^2 - 1}{\bar{\lambda}_{\|}\lambda_{0\|}\bar{\lambda}_{\perp}^2\lambda_{0\perp}^2}\right) + \frac{1}{\bar{\lambda}_{\|}\lambda_{0\|}\bar{\lambda}_{\perp}^2\lambda_{0\perp}^2} + \frac{\chi}{\lambda_{0\|}^2\bar{\lambda}_{\|}^2\bar{\lambda}_{\perp}^4\lambda_{0\perp}^4}\right] \tag{3.7}$$

These equations define $\bar{\lambda}_{\|}$ and $\bar{\lambda}_{\perp}$ implicitly as functions of μ and will appear as constraints in the numerical implementation of our model (see Section 6).

4. Derivation of the governing equations

4.1. Mechanical equilibrium

The material has a target state $\bar{C} = \bar{C}(\mu)$ that it would like to attain in the absence of external forces due to swelling caused by humidity. The elastic part of the strain (i.e., the part that is responsible for increasing the elastic energy with respect to the target state) is the deviation from this state and can be expressed as

$$E = \frac{1}{2}(C - \bar{C}) \tag{4.1}$$

Eq. (2.6) can be written in terms of E, as follows:

$$\widetilde{W}(E) = W(\bar{C}) + \frac{1}{2}\langle \mathbb{C}E, E\rangle \tag{4.2}$$

where we have dropped from the notation the dependence on μ and $\mathbb{C}$ is the fourth order tensor of the elastic moduli; explicit formulas for this tensor are given in Appendix B.

From the expression in Eq. (4.2), using the fact that the integral of this energy is stationary at an equilibrium state, we obtain the equation for mechanical equilibrium

$$\nabla \cdot S = 0 \tag{4.3}$$

where S is the first Piola–Kirchhoff stress tensor, defined by

$$S = FS_c \tag{4.4}$$

where $S_c = \frac{\partial \widetilde{W}}{\partial E} = \mathbb{C}E$ is the Cosserat stress tensor. This is shown in detail in Appendix A. Eq. (4.4) can thus be written as

$$\nabla \cdot (FS_c) = 0 \tag{4.5}$$

which is one of the governing equations for our system, the one expressing mechanical equilibrium. This is coupled with boundary conditions on deformation or stress, as appropriate.

4.2. Diffusion

In this section, we derive the equation governing solvent diffusion; we start from the classical relation that links solvent concentration and the gradient of the chemical potential.

$$\dot{c} = \nabla \cdot (M \nabla \mu) \tag{4.6}$$

Here c is the molar solvent concentration, and M is the mobility tensor which describes how fast the solvent flows.

Solvent and solid are incompressible, but changes in water concentration can cause variations in the system's volume. As a result, the volumetric constraint couples water concentration to system deformation and vice versa. This condition is expressed by

$$JJ_0 = 1 + \Omega J_0 c \tag{4.7}$$

where $J = (\det C)^{\frac{1}{2}}$ is the Jacobian determinant. Taking the derivative of Eq. (4.7) with respect to time leads to

$$\dot{c} = \frac{1}{\Omega}\dot{J} \tag{4.8}$$

By combining Eqs. (4.6), and Eq. (4.8), we get:

$$\Omega\nabla\cdot(M\nabla\mu)=\dot{J}=g\left(\bar{\lambda}_{\parallel},\bar{\lambda}_{\perp},E,\dot{E}\right) \tag{4.9}$$

The RHS of Eq. (4.9) emphasizes that $\dot{J}$ depends solely on $\bar{\lambda}_{\parallel}$, $\bar{\lambda}_{\perp}$, E, and $\dot{E}$. The following explicit expression of $g\left(\bar{\lambda}_{\parallel},\bar{\lambda}_{\perp},E,\dot{E}\right)$ is derived in Appendix A.

$$\begin{aligned} g\left(\bar{\lambda}_{\parallel},\bar{\lambda}_{\perp},E,\dot{E}\right) =& \bar{\lambda}_{\parallel}\bar{\lambda}_{\perp}^{2}\left\{2\left(\bar{\lambda}_{\parallel}^{-2}-\bar{\lambda}_{\perp}^{-2}\right)\left[\bar{\lambda}_{\parallel}^{-1}\dot{\bar{\lambda}}_{\parallel}\left(1-2\left(\bar{\lambda}_{\parallel}^{-2}-\bar{\lambda}_{\perp}^{-2}\right)\right)\right.\right.\\ &\left.\left.-4\bar{\lambda}_{\perp}^{-2}\bar{\lambda}_{\parallel}\dot{\bar{\lambda}}_{\parallel}+2\bar{\lambda}_{\perp}^{-1}\dot{\bar{\lambda}}_{\perp}\right]-2\bar{\lambda}_{\perp}^{-4}\left(2\bar{\lambda}_{\parallel}\dot{\bar{\lambda}}_{\parallel}\right)\right\}(E\cdot A)\\ &+2\bar{\lambda}_{\perp}\left(\bar{\lambda}_{\perp}\dot{\bar{\lambda}}_{\parallel}+2\bar{\lambda}_{\parallel}\dot{\bar{\lambda}}_{\perp}\right)+2\left(\dot{\bar{\lambda}}_{\parallel}+2\bar{\lambda}_{\perp}^{-1}\bar{\lambda}_{\parallel}\dot{\bar{\lambda}}_{\perp}\right)\mathrm{tr}\,E\\ &-4\bar{\lambda}_{\perp}^{-1}\bar{\lambda}_{\parallel}\dot{\bar{\lambda}}_{\perp}(E\cdot P)+2\bar{\lambda}_{\parallel}\bar{\lambda}_{\perp}^{2}\left(\bar{\lambda}_{\parallel}^{-2}A+\bar{\lambda}_{\perp}^{-2}P\right)\cdot\dot{E} \end{aligned} \tag{4.10}$$

Eq. (4.9) is coupled with the boundary condition $\mu=\mu_{ext}$ on $\partial\mathcal{B}$.

5. The case of one passive layer

Our model applies to general bilayers, for which each of the two layers is active, anisotropic, and elastic, as described in the previous sections. A special but biologically relevant example of an active bilayer is one where one layer is anisotropic and active, and the other is passive. For example, the bottom layer can be a passive layer made up of a purely elastic isotropic material for which the elastic energy vanishes in the reference configuration, where the strain $E=0$. We model this passive layer as infinitely permeable to the solvent (infinite mobility $M=\infty$), allowing it to equilibrate to the external chemical potential (μ_{ext}) instantaneously. Thus, the chemical potential at the interface between the two layers has the value ($\mu=\mu_{ext}$). Furthermore, we assume that this passive layer has no coupling between water and mechanics. As a consequence, the mixing part of the energy in Eq. (2.1) will be omitted. The energy expression for the passive layer will then be as follows

$$W(C)=W_{el}(C)=\frac{1}{2}\langle\mathbb{C}E,E\rangle \tag{5.1}$$

The mechanical behavior of this isotropic material is described through the elasticity tensor $\mathbb{C}$, which can be expressed using the isotropic Hooke's law:

$$S_c=\mathbb{C}E=2GE+k(trE)I \tag{5.2}$$

where G is the shear modulus and k is Lamé modulus.

6. Numerical implementation

The model discussed in the previous sections has been implemented and numerically solved in the finite element software COMSOL Multiphysics v5.6. The governing Eqs. (6.2)–(6.4) were implemented using the weak form PDE module. The time-stepping approach employs the implicit adaptive step-size Generalized Alpha (GA) or BDF solver. An iterative quasi-Newton algorithm is used to solve the non-linear algebraic system that emerges from the finite element discretization during each time step. The direct solver MUMPS solves the linearized system at every iteration. The state variables implemented in COMSOL are the deformation f measured from the reference state $\mathcal{B}$ and the chemical potential μ, with $\mathcal{B}$ being the computational domain representing the initial, free-swollen state. The reference configuration of our (symmetric) bilayer structure is denoted by $\mathcal{B}:=[0,L]\times[-\frac{W}{2},\frac{W}{2}]\times[-\frac{H}{2},\frac{H}{2}]\subset\mathbb{R}^3$, where L is the length, W is the total width, and H is the total thickness. Each of the two halves of the bilayer $\mathcal{B}_{top}$ and $\mathcal{B}_{bot}$ has thickness $\frac{H}{2}$. For a point $x\in\mathcal{B}$, we write $x=(x,y,z)$, $x\in[0,L]$, $y\in[-\frac{W}{2},\frac{W}{2}]$, and $z\in[-\frac{H}{2},\frac{H}{2}]$ (see Fig. 2).

First, we impose the relations between $\bar{\lambda}_{0\parallel}$, $\bar{\lambda}_{0\perp}$, and μ_0. While Eq. (3.2) expresses $\bar{\lambda}_{0\perp}$ explicitly in terms of $\bar{\lambda}_{0\parallel}$, Eq. (3.3) is enforced as a constraint between $\bar{\lambda}_{0\parallel}$, $\bar{\lambda}_{0\perp}$, and μ_0. We implement this constraint

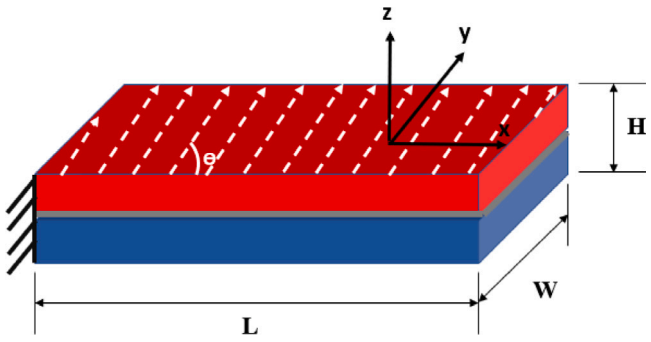

Fig. 2. Reference configuration of the bilayer structure and the global reference frame.

using COMSOL distributed ODEs interface: setting the coefficients of time derivatives to zero, we impose that the source term vanishes, $f=0$, where

$$f=\frac{G\Omega}{\lambda_{0\parallel}}+RT\left[\log\left(\frac{\lambda_{0\parallel}\lambda_{0\perp}^{2}-1}{\lambda_{0\parallel}\lambda_{0\perp}^{2}}\right)+\frac{1}{\lambda_{0\parallel}\lambda_{0\perp}^{2}}+\frac{\chi}{\lambda_{0\parallel}{}^{2}\lambda_{0\perp}^{4}}\right]-\mu_0=0 \tag{6.1}$$

We deal with Eqs. (3.6) and (3.7), enforcing the relations between $\bar{\lambda}_{\parallel}$, $\bar{\lambda}_{\perp}$, and μ, in exactly the same way.

Then, we recast the remaining equations in a weak form. The mechanical equilibrium equation reads:

$$\int_{\mathcal{B}}S_c\cdot\tilde{E}=\int_{\mathcal{B}}FS_c\cdot\nabla\tilde{f}=\int_{\mathcal{B}}S\cdot\nabla\tilde{f}=0 \tag{6.2}$$

where $\tilde{E}$ and $\tilde{f}$ represent test functions, and we use Lagrange quadratic shape functions.

The solvent balance is written in weak form as

$$\int_{\mathcal{B}}h\cdot\nabla\tilde{\mu}-\int_{\beta}g\left(\bar{\lambda}_{\parallel},\bar{\lambda}_{\perp},E,\dot{E}\right)\tilde{\mu}=0 \tag{6.3}$$

where $h=-M\nabla\mu$ is the solvent flux and $\tilde{\mu}$ is a test function (we use Lagrange quadratic shape functions). The boundary condition $\mu=\mu_{\text{ext}}$ is enforced in weak form as

$$\int_{\partial\mathcal{B}}\left(\mu-\mu_{\text{ext}}\right)\tilde{\bar{\lambda}}=0 \tag{6.4}$$

where $\tilde{\bar{\lambda}}$ is a test function (where, again, we use Lagrange quadratic shape functions).

The problem we solved numerically can be summarized as follows: Find the deformation map f, the chemical potential μ on $\mathcal{B}$, and the Lagrange multiplier $\bar{\bar{\lambda}}$ on $\partial\mathcal{B}$ such that the mechanical and chemical equilibrium is satisfied in weak form (Eqs. (6.2)–(6.3)), the external chemical potential has the value μ_{ext} (Eq. (6.4)), one end face of the bilayer is clamped and the rest of its boundary is free.

7. Test cases and discussion of the results

As a showcase of the diversity of motions and shapes that can be obtained with our model, we have selected the case of a bilayer made of one active and one passive layer. We model a system that, in the reference configuration corresponding to the reference chemical potential μ_0, is a straight cantilever. In this straight configuration, the active layer is stress-free and in a state of wetting which is intermediate between the fully wet and the fully dry cases. As a consequence, the bilayer will deform when either drying or further wetting is induced by a change in environmental conditions.

7.1. Equilibrium shapes corresponding to given $\bar{C}$

As a first test case, we consider the simpler problem of computing equilibrium shapes corresponding to a freely assigned target state $\bar{C}$, which is not necessarily achievable by swelling. We assume that $\bar{\lambda}_{\parallel top}=$

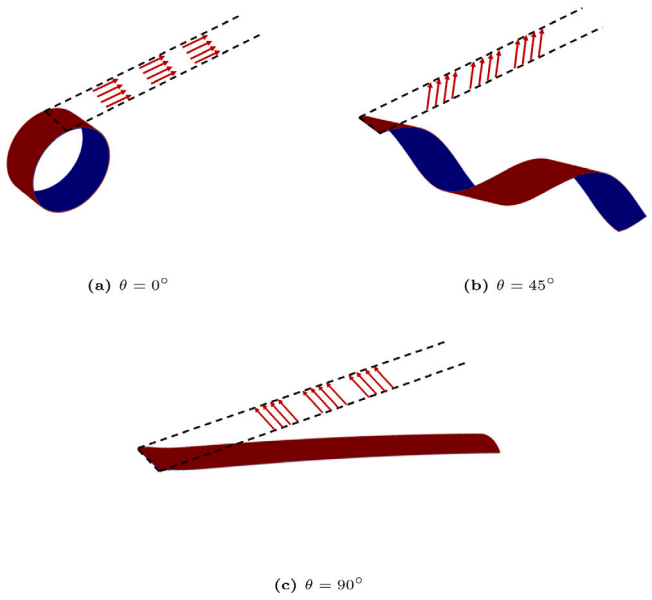

Fig. 3. Variety of motions and shape changes with respect to the reference configuration resulting from different angles θ between fiber orientation and longitudinal axis of the specimen. Here $\bar{\lambda}_{\parallel top} = 1.04$, and $\bar{\lambda}_{\perp top} = \bar{\lambda}_{\parallel bot} = \bar{\lambda}_{\perp bot} = 1$. (For interpretation of the references to color in this figure legend, the reader is referred to the web version of this article.)

1.04 and $\bar{\lambda}_{\perp top} = 1$ (top layer anisotropic and active), and $\bar{\lambda}_{\parallel bot} = \bar{\lambda}_{\perp bot} = 1$ (bottom layer isotropic and passive). These parameters correspond to a material that, upon swelling, would stretch more in the direction parallel to the fibers than in the perpendicular one.

To study the effect of different fiber orientations, we consider the following values for the fiber angle θ between the fiber a and the x-axis: $\theta = 0°$, $\theta = 45°$, and $\theta = 90°$. The corresponding deformed geometries are shown in Fig. 3.

The color pattern in the deformed shapes is just $\bar{\lambda}_{\parallel}$ and it is used to distinguish the top layer (that in this case elongates in the direction of the fiber) from the bottom one. The feature common to all of the panels is that the mid-surface deforms to a cylindrical surface. Of particular interest is the case of the panel (c) in Fig. 3, where the downward global bending of the bilayer is entirely due to the presence of the clamp boundary condition at the constrained end of the cantilever. In fact, in the absence of this constraint, the steady-state equilibrium configuration would consist of a straight cylindrical barrel, with the axis of the cylinder along the longitudinal axis of the specimen. This configuration is incompatible with the prescribed displacements at the clamp, which must all vanish. In order to resolve this conflict, a three-dimensional state of stress is generated at the clamped end, and this results in the downward bending of the structures. Dimensionally-reduced models for the active bilayer (i.e., one-dimensional or two-dimensional models rather than the fully three-dimensional model described here) would be unable to resolve the three-dimensional nature of the mechanical stresses near the clamp and would therefore be unable to predict the global downward bending of the bilayer

7.2. Steady-states at given μ_{ext}

We now move to the problem of finding equilibrium shapes corresponding to a given value of the external chemical potential when the relationship between the principal stretches of the target state and the chemical potential is given by (3.6)–(3.7). We analyze the steady-state configurations that occur as the active layer experiences more wetting or drying, depending on whether the chemical potential increases or decreases relative to the reference value μ_0. At steady state, the chemical potential in the interior of the bilayer has equilibrated to a uniform value, that of the external environment, $\mu = \mu_{ext}$ in $\mathcal{B}$. The target state in the top layer (the only one that is active) is $\bar{C} = \bar{C}(\mu_{ext})$. The corresponding values of $\bar{\lambda}_{\parallel top}(\mu_{ext})$ and $\bar{\lambda}_{\perp top}(\mu_{ext})$ are enforced through the implicit Eqs. (3.6)–(3.7), acting as constraints. The equilibrium configuration corresponding to $\bar{C}(\mu_{ext})$ follows by solving the equilibrium equation (6.2), just like in the previous section. The values for material and geometric parameters used in all the simulations that follow are given in Table 1.

Table 1
Parameter values used in the numerical simulations.

Parameter	Symbol	Value
Anisotropy (top layer)	γ_{top}	0.2
Anisotropy (bottom layer)	γ_{bot}	0
Solvent diffusivity	D	$1 \times 10^{-5}\ \frac{m^2}{s}$
Lamé modulus	k	500 MPa
Shear modulus (top layer) [27]	G_{top}	30 MPa
Shear modulus (bottom layer) [27]	G_{bot}	50 MPa
Universal gas constant	R	$8.134\ \frac{J}{mol\ K}$
Temperature	T	293 K
Flory–Huggins interaction parameter [28]	χ	0.2
Water molar volume	Ω	$1 \times 10^{-5}\ \frac{m^3}{mol}$
Initial chemical potential	μ_0	$-100\ \frac{J}{mol}$
Thickness (top layer)	h_{top}	100 μm
Thickness (bottom layer)	h_{bot}	100 μm
Width	W	5 mm
Length	L	50 mm

First, we examine the hygroscopic behavior of the material in the wetting situation ($\mu_{ext} > \mu_0$) when the external chemical potential (μ_{ext}) increases from $\mu = -100\frac{J}{mol}$ to $\mu = -30\frac{J}{mol}$. Fig. 4 illustrates a situation similar to Fig. 3, namely, further wetting from an initial state of intermediate wetting. The difference is that, now, the active material elongates upon wetting along the direction perpendicular to the fibers more than along the fibers because it is assumed that the fibers are more resistant to stretching than the surrounding matrix (see, e.g., (3.2) and recall that the anisotropy parameter γ has been assumed positive). The color patterns in the deformed shapes refer to the moisture content in the top layer (specifically, the ratio between the steady-state concentration c and the concentration c_0 in the initial configuration). Ratios larger than 1 indicate moisture absorption with respect to the initial, partially wet state. Only the top active layer is shown in this figure and in the following ones.

Then, we investigate the coiling motions caused by decreasing the humidity in the surrounding environment starting from a partially wet state. We test the drying behavior for a particular angle ($\theta = 75°$), which is motivated by studies of the coiling behavior of natural seeds in Abraham et al. [25]. The data show that the fiber of the seeds is at an angle range between 70° and 80°. The chemical potential is reduced from $\mu = -100\frac{J}{mol}$ to $\mu = -350\frac{J}{mol}$. The panels have different configurations resulting from different choices for the width W, while all other material and geometric parameters are kept constant. As the external humidity decreases, the structure will shrink, with the orange outer layer representing the deformed configuration of the active top layer. This shrinking will occur perpendicular to the fibers and induce twisting and bending, resulting in spontaneous curvature and torsion of the layer midline. For small enough W we obtain a helix with a narrow pitch. When W is too large, the layer coils onto itself, overlapping at each new turn. To resolve correctly the outer radius of this and similar cylindrical geometries, such as the ones of Figs. 3(a) and 4(a), we would need to include the effects of self-contact in our model, see e.g. [26]. We show, nevertheless, these (slightly) unrealistic geometries in Fig. 5(b), for comparison with Fig. 5(a).

7.3. Transient states

We describe the transient states corresponding to varying the chemical potential of the environment from μ_0 to μ_{ext}. The initial state of the

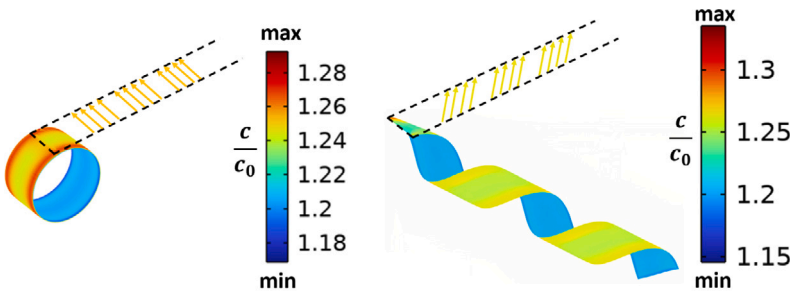

(a) $\theta = 90^\circ \quad \gamma_{top} = 0.2 \quad \gamma_{bot} = 0$ (b) $\theta = 45^\circ \quad \gamma_{top} = 0.2 \quad \gamma_{bot} = 0$

Fig. 4. Steady state geometries and solvent concentration relative to the initial value c_0 for further wetting with respect to an initial, partially wet state; two different angles θ between fiber orientation and longitudinal axis of the specimen are shown in the two panels. Only the top active layer is shown. (For interpretation of the references to color in this figure legend, the reader is referred to the web version of this article.)

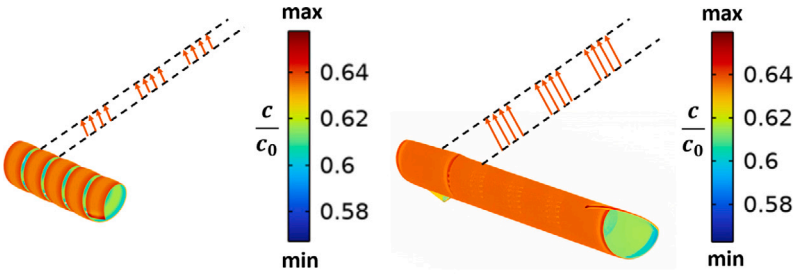

(a) $\theta = 75^\circ \quad W = 5$ mm (b) $\theta = 75^\circ \quad W = 1.75$ mm

Fig. 5. Steady state geometries and solvent concentration relative to the initial value c_0 for a drying experiment starting from an initial, partially wet state; different widths lead to different configurations characterized by different degree of overlapping between successive coils. Only the top active layer is shown.

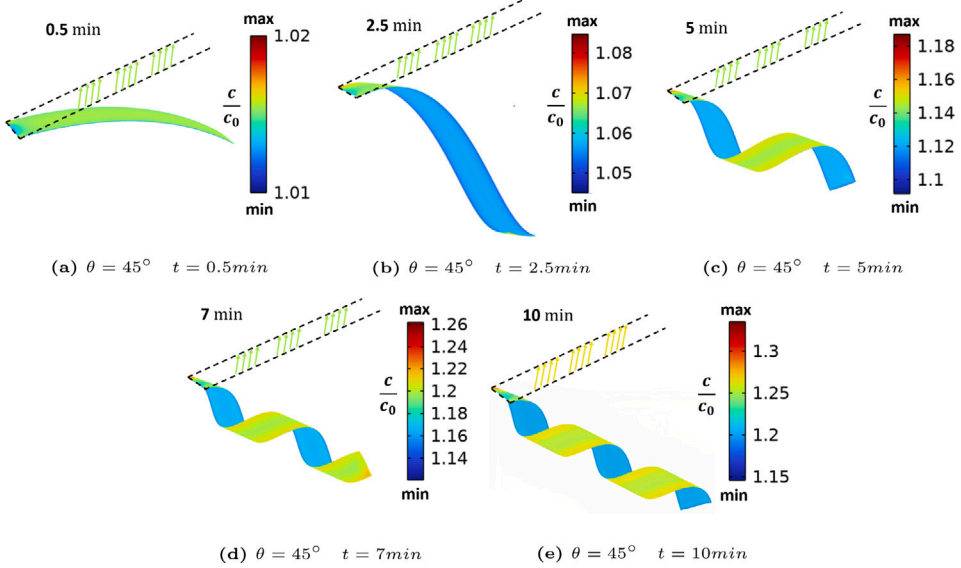

(a) $\theta = 45^\circ \quad t = 0.5min$ (b) $\theta = 45^\circ \quad t = 2.5min$ (c) $\theta = 45^\circ \quad t = 5min$

(d) $\theta = 45^\circ \quad t = 7min$ (e) $\theta = 45^\circ \quad t = 10min$

Fig. 6. Representative snapshots showing time-resolved coiling upon swelling for fiber angle $\theta = 45^\circ$ when the external chemical potential (μ_{ext}) increases from $\mu = -100\frac{\text{J}}{\text{mol}}$ to $\mu = -30\frac{\text{J}}{\text{mol}}$ with steady rate of change over 10 min. Only the top active layer is shown.

system is described by $\mu = \mu_0$ in $\mathcal{B}$ and $C = I = \bar{C}(\mu_0)$. Then, we change μ_{ext} with a prescribed time ramp, e.g., at a constant rate, and impose the BC $\mu = \mu_{ext}$ at $\partial\mathcal{B}$. The chemical potential at points inside the bilayer $\mathcal{B}$ (or inside the active part of the bilayer if only one layer is active, say $\mathcal{B}_{top}$) evolves from the initial state μ_0 to the final equilibrium value $\mu = \mu_{ext}$, constant throughout the body (or throughout $\mathcal{B}_{top}$). During the transient in which μ_{ext} varies from the initial to the final value, the chemical potential in the active layer $\mu(x,t)$ varies in space and time so that also the target state of the material $\bar{C} = \bar{C}(\mu(x,t))$ evolves in time and space.

Figs. 6 and 7 show representative examples of slow time-dependent evolutions through (quasi-equilibrium) transient states. In the first figure, as the external chemical potential (μ_{ext}) increases from $\mu = -100\frac{\text{J}}{\text{mol}}$ to $\mu = -30\frac{\text{J}}{\text{mol}}$ with a slow, steady rate of change over 10 min,

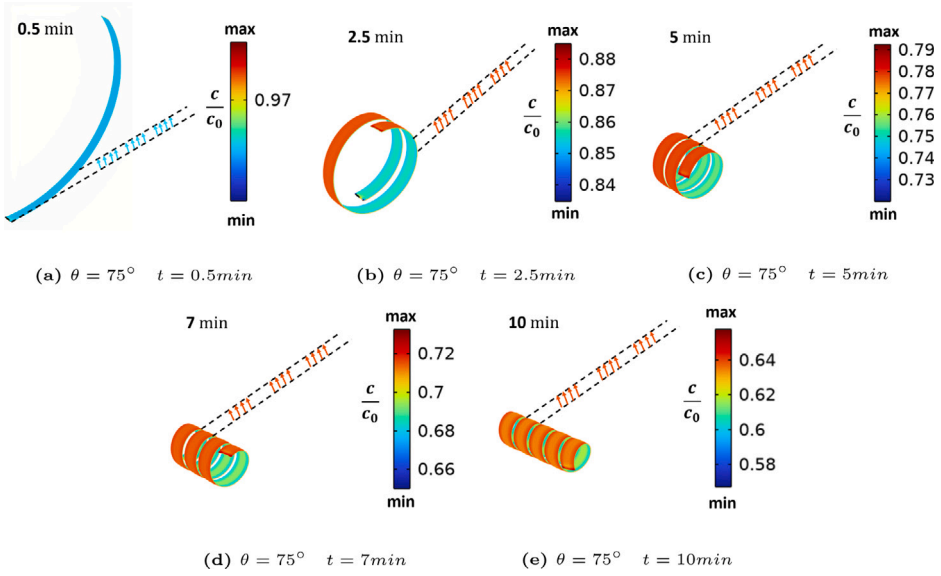

(a) $\theta = 75^\circ \quad t = 0.5min$ (b) $\theta = 75^\circ \quad t = 2.5min$ (c) $\theta = 75^\circ \quad t = 5min$

(d) $\theta = 75^\circ \quad t = 7min$ (e) $\theta = 75^\circ \quad t = 10min$

Fig. 7. Representative snapshots showing time-resolved coiling upon shrinking for fiber angle $\theta = 75^\circ$ when the external chemical potential (μ_{ext}) declines from $\mu = -100\frac{\text{J}}{\text{mol}}$ to $\mu = -350\frac{\text{J}}{\text{mol}}$ with steady rate of change over 10 min. Only the top active layer is shown.

the active layer swells as it progressively wets, and the bilayer bends. The fiber angle is $\theta = 45°$, and the configuration finally converges to the steady state shown in Fig. 4(b).

In the other figure, when (μ_{ext}) decrease from $\mu = -100\frac{\text{J}}{\text{mol}}$ to $\mu = -350\frac{\text{J}}{\text{mol}}$ over the same period, the top active layer shrinks and dries, and the configuration eventually converges to the steady state shown in Fig. 5(a).

8. Conclusion

In this work, we have developed a three-dimensional model for the coupled evolution of elastic deformations and moisture content for an elastic soft hygroscopic bilayer. The system of governing equations for mechanical equilibrium and chemical diffusion has been deduced based on the use of the Flory–Rehner model to describe the free energy of a hygroscopic material. This model has then been implemented in COMSOL Multiphysics using weak formulations to characterize the bilayer's equilibrium and transient shapes.

The model was able to simulate the wide variety of equilibrium configurations exhibited by bilayer structures at a steady state. In particular, when only the top layer is active, while the bottom one is passive and isotropic, different shapes (circular roll, helical structures with curvature and torsion of the midline, cylindrical barrel) are observed in correlation to different fiber orientations. The steady configurations we have obtained and the transient states traversed to reach the final configuration are qualitatively similar to the ones typically observed in natural and artificial systems. Finally, realistic shapes for the coiling behavior induced by drying can be attained by tuning the width value, which determines the degree of overlapping in the structure as coiling proceeds.

While our results are mainly of a qualitative nature, they show the consequences on the morphed shapes of a specific choice of material parameters (such as the orientation of the fibers and their stiffness), geometry (such as the width vs. thickness or width vs. length ratios), and mechanical constraints (such as the role of the clamp in Fig. 3(c)). These restrictions on the morphed shapes that can be obtained may prove helpful in the design of artificial motile hygromorphic bilayers.

Future work will explore more fully the dependence of achievable steady shapes and shape evolution on the material and geometric parameters, also in the presence of external forces and environmental constraints that may oppose and hinder the hygroscopic shape changes.

Declaration of competing interest

The authors declare the following financial interests/personal relationships which may be considered as potential competing interests: The authors report financial support was provided by the European Union's Horizon 2020 Research and Innovation Programme under Grant Agreement No 101017940 (I-Seed). ADS is a member of the INdAM Research Group GNFM.

Data availability

Data will be made available on request

Acknowledgments

This work has received funding from the European Union's Horizon 2020 Research and Innovation Programme under Grant Agreement No 101017940 (I-Seed). ADS is a member of the INdAM Research Group GNFM.

Appendix A. Details on reference and target states, derivation of governing equations

A.1. Reference and target state

We start by taking the derivative $\frac{\partial W}{\partial C}$ of Eq. (2.1)

$$\begin{aligned}\frac{\partial W}{\partial C}(C,\mu) = &\frac{1}{(\det C_0)^{1/2}}\frac{G}{2}\left[F_0F_0^T + 2\gamma\left(I_4(C)-1\right)F_0a\otimes F_0a\right]\\ &+\frac{1}{2}(\det C)^{\frac{1}{2}}\left(W'_{mix}\left((\det C)^{\frac{1}{2}}\right)-\frac{\mu}{\Omega}\right)C^{-1}\end{aligned} \tag{A.1}$$

where $I_4 = \left|FF_0a\right|^2 = FF_0a\cdot FF_0a = F_0^TCF_0\cdot a\otimes a$.

Then, we impose that the reference state $C = I = \bar{C}(\mu_0)$ minimizes the free energy at fixed $\mu = \mu_0$

$$\left.\frac{\partial W}{\partial C}(C,\mu_0)\right|_{C=\bar{C}_0(\mu_0)=I} = 0 \tag{A.2}$$

Similarly, we impose that the target state $C = \bar{C}(\mu)$ minimizes the free energy at fixed μ

$$\left.\frac{\partial W}{\partial C}(C,\mu)\right|_{C=\bar{C}(\mu)} = 0 \tag{A.3}$$

By symmetry, setting $A = a \otimes a$ and $P = I - a \otimes a$, we have:

$$F_0 = \lambda_{0\parallel} A + \lambda_{0\perp} P \tag{A.4}$$

and

$$F_0^T F_0 = \lambda_{0\parallel}^2 A + \lambda_{0\perp}^2 P \tag{A.5}$$

so that

$$det(F_0^T F_0) = \lambda_{0\parallel}^2 \lambda_{0\perp}^4 \tag{A.6}$$

Correspondingly, the symmetry properties in the target state imply

$$\bar{C}(\mu) = \bar{\lambda}_\parallel^2 A + \bar{\lambda}_\perp^2 P \tag{A.7}$$

Using Eq. (A.5), we can write the first derivative of the mixing energy (W'_{mix}) as follows

$$W'_{mix}(\det C)^{\frac{1}{2}}|_{C=I} = \frac{RT}{\Omega}\left[\log\left(\frac{\lambda_{0\parallel}\lambda_{0\perp}^2 - 1}{\lambda_{0\parallel}\lambda_{0\perp}^2}\right) + \frac{1}{\lambda_{0\parallel}\lambda_{0\perp}^2} + \frac{\chi}{\lambda_{0\parallel}^2\lambda_{0\perp}^4}\right] \tag{A.8}$$

Then, substituting Eq. (A.5) in (A.2), we obtain

$$\begin{aligned}\frac{\partial W}{\partial C}(I,\mu_0) =& \frac{1}{(\det C_0)^{1/2}}\frac{G}{2}\left[F_0 F_0^T + 2\gamma\left(I_4 - 1\right)F_0 a \otimes F_0 a\right] \\ &+ \frac{1}{2}(\det I)^{\frac{1}{2}}\left(W'_{mix}\left((\det I)^{\frac{1}{2}}\right) - \frac{\mu_0}{\Omega}\right)I^{-1} = 0\end{aligned} \tag{A.9}$$

By pre-multiplying Eq. (A.9) by F_0^T and post-multiplying it by F_0^{-T} we obtain, after rearrangements,

$$\frac{F_0^T F_0}{\left(det\left(F_0^T F_0\right)\right)^{1/2}}[I + 2\tilde{\gamma}(a \otimes a)] = -\frac{1}{G}\left(W'_{mix}(1) - \frac{\mu_0}{\Omega}\right)I \tag{A.10}$$

where $\tilde{\gamma} = \gamma\left(F_0^T F_0 \cdot a \otimes a - 1\right)$. We then multiply Eq. (A.10) by $A = a \otimes a$ and obtain

$$\begin{aligned}\mu_0 =& \frac{G\Omega}{\lambda_{0\parallel}\lambda_{0\perp}^2}\left[\lambda_{0\parallel}^2 + 2\gamma\left(\lambda_{0\parallel}^2 - 1\right)\lambda_{0\parallel}^2\right] + RT \\ &\left[\log\left(\frac{\lambda_{0\parallel}\lambda_{0\perp}^2 - 1}{\lambda_{0\parallel}\lambda_{0\perp}^2}\right) + \frac{1}{\lambda_{0\parallel}\lambda_{0\perp}^2} + \frac{\chi}{\lambda_{0\parallel}^2\lambda_{0\perp}^4}\right]\end{aligned} \tag{A.11}$$

Moreover, we multiply Eq. (A.10) by $P = I - a \otimes a$ and obtain

$$\mu_0 = \frac{G\Omega}{\lambda_{0\parallel}} + RT\left[\log\left(\frac{\lambda_{0\parallel}\lambda_{0\perp}^2 - 1}{\lambda_{0\parallel}\lambda_{0\perp}^2}\right) + \frac{1}{\lambda_{0\parallel}\lambda_{0\perp}^2} + \frac{\chi}{\lambda_{0\parallel}^2\lambda_{0\perp}^4}\right] \tag{A.12}$$

Eqs. (3.6) and (3.7) are obtained in a similar way. By substituting Eq. (A.7) in Eq. (A.3), we get

$$\begin{aligned}&\frac{1}{\lambda_{0\parallel}\lambda_{0\perp}^2}G\left[\lambda_{0\parallel}^2 A + \lambda_{0\perp}^2 P_\perp + 2\gamma\left(\lambda_{0\parallel}^2\bar{\lambda}_\parallel^2 - 1\right)\lambda_{0\parallel}^2 A\right] + \left(\bar{\lambda}_\parallel\bar{\lambda}_\perp^2\right) \\ &\left\{RT\left[\log\left(\frac{\bar{\lambda}_\parallel\lambda_{0\parallel}\bar{\lambda}_\perp^2\lambda_{0\perp}^2 - 1}{\bar{\lambda}_\parallel\lambda_{0\parallel}\bar{\lambda}_\perp^2\lambda_{0\perp}^2}\right) + \frac{1}{\bar{\lambda}_\parallel\lambda_{0\parallel}\bar{\lambda}_\perp^2\lambda_{0\perp}^2} + \frac{\chi}{\lambda_{0\parallel}^2\bar{\lambda}_\parallel^2\bar{\lambda}_\perp^4\lambda_{0\perp}^4}\right]\right. \\ &\left.-\frac{\mu}{\Omega}\right\}\left(\bar{\lambda}_\parallel^{-2}A + \bar{\lambda}_\perp^{-2}P_\perp\right) = 0\end{aligned} \tag{A.13}$$

Multiplying Eq. (A.13) by $A = a \otimes a$ we get

$$\begin{aligned}\mu =& \frac{\bar{\lambda}_\parallel\lambda_{0\parallel}}{\bar{\lambda}_\perp^2\lambda_{0\perp}^2}G\Omega\left[1 + 2\gamma\left(\lambda_{0\parallel}^2\bar{\lambda}_\parallel^2 - 1\right)\right] \\ &+ RT\left[\log\left(\frac{\bar{\lambda}_\parallel\lambda_{0\parallel}\bar{\lambda}_\perp^2\lambda_{0\perp}^2 - 1}{\bar{\lambda}_\parallel\lambda_{0\parallel}\bar{\lambda}_\perp^2\lambda_{0\perp}^2}\right) + \frac{1}{\bar{\lambda}_\parallel\lambda_{0\parallel}\bar{\lambda}_\perp^2\lambda_{0\perp}^2} + \frac{\chi}{\lambda_{0\parallel}^2\bar{\lambda}_\parallel^2\bar{\lambda}_\perp^4\lambda_{0\perp}^4}\right]\end{aligned} \tag{A.14}$$

Finally, multiplying Eq. (A.13) by $P = I - a \otimes a$ we get

$$\begin{aligned}\mu =& \frac{G\Omega}{\bar{\lambda}_\parallel\lambda_{0\parallel}} + RT\left[\log\left(\frac{\bar{\lambda}_\parallel\lambda_{0\parallel}\bar{\lambda}_\perp^2\lambda_{0\perp}^2 - 1}{\bar{\lambda}_\parallel\lambda_{0\parallel}\bar{\lambda}_\perp^2\lambda_{0\perp}^2}\right) + \frac{1}{\bar{\lambda}_\parallel\lambda_{0\parallel}\bar{\lambda}_\perp^2\lambda_{0\perp}^2}\right. \\ &\left.+ \frac{\chi}{\lambda_{0\parallel}^2\bar{\lambda}_\parallel^2\bar{\lambda}_\perp^4\lambda_{0\perp}^4}\right]\end{aligned} \tag{A.15}$$

A.2. Mechanical equilibrium

In this part, we derive the mechanical equilibrium equations. We can write the strain equation as follows

$$E(f) = \frac{1}{2}\left(\nabla f^T \nabla f - \bar{C}\right) \tag{A.16}$$

so that

$$\begin{aligned}E(f + t\delta f) =& \frac{1}{2}\left(\nabla f^T \nabla f - \bar{C}\right) + \frac{1}{2}\left(\nabla f^T \nabla \delta f + \nabla f(\nabla \delta f)^T\right)t \\ &+ \frac{1}{2}\left((\nabla \delta f)^T \nabla f\right)t^2\end{aligned} \tag{A.17}$$

We impose the condition that the integral of the energy,

$$\mathcal{E}(f) = \int_{\mathcal{B}} \widetilde{W}(E(f)) \tag{A.18}$$

where $\widetilde{W}$ is given by (4.2), is stationary at f (at fixed μ) as follows

$$\begin{aligned}\frac{d\mathcal{E}}{dt}(f + t\delta f)\Big|_{t=0} &= \int_{\mathcal{B}} \frac{\partial \widetilde{W}}{\partial E}(E(f)) \cdot \frac{d}{dt}E(f + t\delta f)\Big|_{t=0} \\ &= \int_{\mathcal{B}} \mathbb{C}E(f) \cdot sym\left(\nabla f^T \nabla \delta f\right)\end{aligned} \tag{A.19}$$

where we have used that $\frac{\partial \widetilde{W}}{\partial E} = \mathbb{C}E(f)$ and $\frac{dE}{dt}(f + t\delta f)\Big|_{t=0} = sym\left(\nabla f^T \nabla \delta f\right)$ which follows by taking the derivative at $t = 0$ in the expression (A.17)

$$\frac{dE}{dt}(f + t\delta f)\Big|_{t=0} = \frac{1}{2}\left(\nabla f^T \nabla \delta f + \nabla f(\nabla \delta f)^T\right) = sym\left(\nabla f^T \nabla \delta f\right) \tag{A.20}$$

Since $\mathbb{C}E(f)$ is symmetric, Eq. (A.19) can be rewritten as

$$\int_{\mathcal{B}} \mathbb{C}E(f) \cdot \nabla f^T \delta f = \int_{\mathcal{B}} F\mathbb{C}E \cdot \nabla \delta f = 0 \tag{A.21}$$

which is the weak form of Eq. (4.3) because $F\mathbb{C}E = FS_c = S$.

A.3. Diffusion

In this part, we show the derivation of the term $g\left(\bar{\lambda}_\parallel, \bar{\lambda}_\perp, E, \dot{E}\right)$ in the RHS of the diffusion Eq. (4.9) in Section 4.2. First, we take the time derivative of the solvent concentration:

$$\begin{aligned}\dot{c} =& \frac{\dot{J}}{\Omega} = \frac{1}{\Omega}\left((\det C)^{1/2}\right)^{\cdot} = \frac{1}{2\Omega}(\det C)^{-\frac{1}{2}}\,\mathrm{cof}\,C \cdot \dot{C} \\ &= \frac{1}{2\Omega}(\det C)^{\frac{1}{2}}C^{-1} \cdot \dot{C}\end{aligned} \tag{A.22}$$

We then substitute the relation between the target state and the strain $C = \bar{C} + 2E$ in Eq. (A.22), and compute the Taylor expansion at order 2

$$\begin{aligned}(\det C)^{\frac{1}{2}}C^{-1} \cdot \dot{C} =& (\det \bar{C})^{\frac{1}{2}}\left\{\bar{C}^{-1}\left[I - 2E\bar{C}^{-1} + \mathrm{tr}\left(\bar{C}^{-1}E\right)I\right]\right. \\ &\left.\cdot\dot{\bar{C}} + 2\bar{C}^{-1} \cdot \dot{E}\right\} + H.O.T.\end{aligned} \tag{A.23}$$

From the symmetry properties of the anisotropic material, we get

$$\dot{\bar{C}} = 2\bar{\lambda}_\parallel\dot{\bar{\lambda}}_\parallel A + 2\bar{\lambda}_\perp\dot{\bar{\lambda}}_\perp P \tag{A.24}$$

and

$$\bar{C}^{-1} = \bar{\lambda}_\parallel^{-1}A + \bar{\lambda}_\perp^{-1}P \tag{A.25}$$

For simplicity, we will divide Eq. (A.23) into parts and use the relations in Eqs. (A.24) and (A.25) in all parts. The first part is $\bar{C}^{-1}E\bar{C}^{-1}$ which could be written as:

$$\bar{C}^{-1}E\bar{C}^{-1} = \left(\lambda_\parallel^{-2}A + \lambda_\perp^{-2}P\right)E\left(\lambda_\parallel^{-2}A + \lambda_\perp^{-2}P\right) \tag{A.26}$$

The following four equations can be used to simplify Eq. (A.23)

$$AEP = AE(I - A) = AE - AEA = AE - (E \cdot A)A \tag{A.27}$$

$$AEA = (a\otimes a)E(a\otimes a) = (a\otimes a)(Ea\otimes a) = (Ea\cdot a)a\otimes a = (Ea\cdot a)A = (E\cdot A)A \tag{A.28}$$

$$PEA = (I - A)EA = EA - AEA = EA - (E \cdot A)A \tag{A.29}$$

$$PEP = (I - A)E(I - A) = E - AE - EA + AEA \tag{A.30}$$

Using the above relations, we can write Eq. (A.26) as follows:

$$\begin{aligned}\bar{C}^{-1}E\bar{C}^{-1} = {} & \bar{\lambda}_{\parallel}^{-4}(E \cdot A)A + \bar{\lambda}_{\parallel}^{-2}\bar{\lambda}_{\perp}^{-2}[2\,\mathrm{sym}(AE) - 2(E \cdot A)A] \\ & + \bar{\lambda}_{\perp}^{-4}[E - 2\,\mathrm{sym}(AE) + (E \cdot A)A]\end{aligned} \tag{A.31}$$

The part $\mathrm{tr}\left(\bar{C}^{-1}E\right)$ from Eq. (A.23) is written as:

$$\begin{aligned}\mathrm{tr}\left(\bar{C}^{-1}E\right) &= \mathrm{tr}\left[\left(\bar{\lambda}_{\parallel}^{-2}A + \bar{\lambda}_{\perp}^{-2}P\right)E\right] = \mathrm{tr}\left(\bar{\lambda}_{\parallel}^{-2}AE\right) + \mathrm{tr}\left(\bar{\lambda}_{\perp}^{-2}PE\right) \\ &= \mathrm{tr}\left(\bar{\lambda}_{\parallel}^{-2}a \otimes Ea\right) + \mathrm{tr}\left(\bar{\lambda}_{\perp}^{-2}(E - AE)\right) \\ &= \bar{\lambda}_{\parallel}^{-2}E \cdot A + \bar{\lambda}_{\perp}^{-2}[\mathrm{tr}\,E - \mathrm{tr}\,EA] \\ &= \left(\bar{\lambda}_{\parallel}^{-2} - \bar{\lambda}_{\perp}^{-2}\right)E \cdot A + \bar{\lambda}_{\perp}^{-2}\,\mathrm{tr}\,E\end{aligned} \tag{A.32}$$

By collecting Eqs. (A.31) and (A.32) we could write $\left[1 + \mathrm{tr}\left(\bar{C}^{-1}E\right)\right]C^{-1} - 2\bar{C}^{-1}E\bar{C}^{-1}$ as shown below:

$$\begin{aligned}\left[1 + \mathrm{tr}\left(\bar{C}^{-1}E\right)\right]C^{-1} - 2\bar{C}^{-1}E\bar{C}^{-1} = {} & \left[1 + \left(\bar{\lambda}_{\parallel}^{-2} - \bar{\lambda}_{\perp}^{-2}\right)E \cdot A + \bar{\lambda}_{\perp}^{-2}\,\mathrm{tr}\,E\right] \\ & \left(\bar{\lambda}_{\parallel}^{-2}A + \bar{\lambda}_{\perp}^{-2}P\right) - 2\bar{\lambda}_{\parallel}^{-4}(E \cdot A)A - 2\bar{\lambda}_{\parallel}^{-2}\bar{\lambda}_{\perp}^{-2} \\ & [2\,\mathrm{sym}(AE) - 2(E \cdot A)A] - 2\bar{\lambda}_{\perp}^{-4}[E - 2\,\mathrm{sym}(AE) \\ & + (E \cdot A)A] \\ = {} & \left\{\left[1 + \left(\bar{\lambda}_{\parallel}^{-2} - \bar{\lambda}_{\perp}^{-2}\right)(E \cdot A) + \bar{\lambda}_{\perp}^{-2}\,\mathrm{tr}\,E\right]\bar{\lambda}_{\parallel}^{-2}\right. \\ & \left. -2\bar{\lambda}_{\parallel}^{-4}(E \cdot A) + 4\bar{\lambda}_{\parallel}^{-2}\bar{\lambda}_{\perp}^{-2}(E \cdot A) - 2\bar{\lambda}_{\perp}^{-4}(E \cdot A)\right\}A \\ & + \left[1 + \left(\bar{\lambda}_{\parallel}^{-2} - \bar{\lambda}_{\perp}^{-2}\right)(E \cdot A) + \bar{\lambda}_{\perp}^{-2}\,\mathrm{tr}\,E\right]\bar{\lambda}_{\perp}^{-2}P - 2 \\ & \left(\bar{\lambda}_{\parallel}^{-2}\bar{\lambda}_{\perp}^{-2} - \bar{\lambda}_{\perp}^{-4}\right)2\,\mathrm{sym}(AE) - 2\bar{\lambda}_{\perp}^{-4}E\end{aligned} \tag{A.33}$$

Multiplying Eq. (A.33) by $\dot{\bar{C}}$ we then obtain

$$\begin{aligned}\left(\left[1 + \mathrm{tr}\left(\bar{C}^{-1}E\right)\right]\bar{C}^{-1} - 2\bar{C}^{-1}E\bar{C}^{-1}\right) \cdot \dot{\bar{C}} = {} & \left\{\left[1 + \left(\bar{\lambda}_{\parallel}^{-2} - \bar{\lambda}_{\perp}^{-2}\right)(E \cdot A)\right.\right. \\ & \left.\left. + \bar{\lambda}_{\perp}^{-2}\,\mathrm{tr}\,E\right]\bar{\lambda}_{\parallel}^{-2} - 2\bar{\lambda}_{\parallel}^{-4}(E \cdot A) + 4\bar{\lambda}_{\parallel}^{-2}\bar{\lambda}_{\perp}^{-2}(E \cdot A)\right. \\ & \left. -2\bar{\lambda}_{\perp}^{-4}(E \cdot A)\right\}2\bar{\lambda}_{\parallel}\dot{\bar{\lambda}}_{\parallel} + \left[1 + \left(\bar{\lambda}_{\parallel}^{-2} - \bar{\lambda}_{\perp}^{-2}\right)(E \cdot A)\right. \\ & \left. + \bar{\lambda}_{\perp}^{-2}\,\mathrm{trE}\right]4\bar{\lambda}_{\perp}^{-2}\dot{\bar{\lambda}}_{\perp}\bar{\lambda}_{\perp} - 2\left(\bar{\lambda}_{\parallel}^{-2}\bar{\lambda}_{\perp}^{-2} - \bar{\lambda}_{\perp}^{-4}\right) \\ & \left(4\bar{\lambda}_{\parallel}\dot{\bar{\lambda}}_{\parallel}E \cdot A\right) - 2\bar{\lambda}_{\perp}^{-4}\left(2\bar{\lambda}_{\parallel}\dot{\bar{\lambda}}_{\parallel}E \cdot A + 2\bar{\lambda}_{\perp}\dot{\bar{\lambda}}_{\perp}E \cdot P\right)\end{aligned} \tag{A.34}$$

Finally, collecting Eq. (A.34) and the remaining part in Eq. (A.23) we can write $g\left(\bar{\lambda}_{\parallel}, \bar{\lambda}_{\perp}, E, \dot{E}\right)$ as follows:

$$\begin{aligned}g\left(\bar{\lambda}_{\parallel}, \bar{\lambda}_{\perp}, E, \dot{E}\right) = {} & (\det \bar{C})^{\frac{1}{2}}\left\{\bar{C}^{-1}\left[I - 2E\bar{C}^{-1} + \mathrm{tr}\left(\bar{C}^{-1}E\right)I\right] \cdot \dot{\bar{C}}\right. \\ & \left. + 2\bar{C}^{-1} \cdot \dot{E}\right\} \\ = {} & \bar{\lambda}_{\parallel}\bar{\lambda}_{\perp}^{2}\left\{\left[\bar{\lambda}_{\parallel}^{-2}\left(\bar{\lambda}_{\parallel}^{-2} - \bar{\lambda}_{\perp}^{-2} - 2\bar{\lambda}_{\parallel}^{-4} + 4\bar{\lambda}_{\parallel}^{-2}\bar{\lambda}_{\perp}^{-2} - 2\bar{\lambda}_{\perp}^{-4}\right)\right.\right. \\ & 2\bar{\lambda}_{\parallel}\dot{\bar{\lambda}}_{\parallel} + \left(\bar{\lambda}_{\parallel}^{-2} - \bar{\lambda}_{\perp}^{-2}\right)4\bar{\lambda}_{\perp}^{-1}\dot{\bar{\lambda}}_{\perp} - 2\bar{\lambda}_{\perp}^{-2}\left(\bar{\lambda}_{\parallel}^{-2} - \bar{\lambda}_{\perp}^{-2}\right)4\bar{\lambda}_{\parallel}\dot{\bar{\lambda}}_{\parallel} \\ & \left.\left. -2\bar{\lambda}_{\perp}^{-4}\left(2\bar{\lambda}_{\parallel}\dot{\bar{\lambda}}_{\parallel}\right)\right](E \cdot A) + \left[2\bar{\lambda}_{\parallel}^{-2}\bar{\lambda}_{\parallel}\dot{\bar{\lambda}}_{\parallel} + 4\bar{\lambda}_{\perp}^{-2}\bar{\lambda}_{\perp}\dot{\bar{\lambda}}_{\perp}\right] \\ & + \left(2\bar{\lambda}_{\perp}^{-2}\bar{\lambda}_{\parallel}^{-2}\bar{\lambda}_{\parallel}\dot{\bar{\lambda}}_{\parallel} + 4\bar{\lambda}_{\perp}^{-4}\bar{\lambda}_{\perp}\dot{\bar{\lambda}}_{\perp}\right)\mathrm{tr}\,E - 4\bar{\lambda}_{\perp}^{-4}\bar{\lambda}_{\perp}\dot{\bar{\lambda}}_{\perp}E \cdot P \\ & +2\left(\bar{\lambda}_{\parallel}^{-2}A + \bar{\lambda}_{\perp}^{-2}P\right) \cdot \dot{E}\right\}\end{aligned} \tag{A.35}$$

Appendix B. Derivation of the elastic stiffness tensor $\mathbb{C}$ from the energy expression

We will now calculate the elastic moduli that characterize the quadratic energy expression written in terms of E as in Eq. (2.6). We can write $\mathbb{C}$ as follows:

$$\begin{aligned}\mathbb{C}(\mu) = {} & 4\frac{\partial^2 W}{\partial C \otimes \partial C}\Big|_{C=\bar{C}(\mu)} \\ = {} & \frac{1}{(\det C_0)^{1/2}}\gamma G\left(F_0 a \otimes F_0 a\right) \otimes \left(F_0 a \otimes F_0 a\right) \\ & + \left(\left((\det C)^{\frac{1}{2}}W'_{mix}\left((\det C)^{\frac{1}{2}}\right) - \frac{\mu}{\Omega}\right) + (\det C)^{\frac{1}{2}}\right. \\ & \left. W''_{mix}\left((\det C)^{\frac{1}{2}}\right)\right)\bar{C}^{-1} \otimes \bar{C}^{-1} - 2(\det C)^{1/2} \\ & \left(W'_{mix}(\det C)^{\frac{1}{2}}\right) - \frac{\mu}{\Omega}\right)\bar{C}^{-1} \boxtimes \bar{C}^{-1}\end{aligned} \tag{B.1}$$

where, for given second-order tensors A, B we are defining the fourth-order tensors $A \otimes B$ and $A \boxtimes B$ through the identities

$$(A \otimes B)U = (B \cdot U)A \tag{B.2}$$

and

$$(A \boxtimes B)U = AUB^T \tag{B.3}$$

holding for every U.

We can write each of the two expressions $\bar{C}^{-1} \otimes \bar{C}^{-1}$ and $\bar{C}^{-1} \boxtimes \bar{C}^{-1}$ as a function of A and P using the tensor product properties as

$$\bar{C}^{-1} \otimes \bar{C}^{-1} = \bar{\lambda}_{\parallel}^{-4}A \otimes A + \bar{\lambda}_{\parallel}^{-2}\bar{\lambda}_{\perp}^{-2}(A \otimes P + P \otimes A) + \bar{\lambda}_{\perp}^{-4}P \otimes P \tag{B.4}$$

and

$$\bar{C}^{-1} \boxtimes \bar{C}^{-1} = \bar{\lambda}_{\parallel}^{-4}A \boxtimes A + \bar{\lambda}_{\parallel}^{-2}\bar{\lambda}_{\perp}^{-2}(A \boxtimes P + P \boxtimes A) + \bar{\lambda}_{\perp}^{-4}P \boxtimes P \tag{B.5}$$

Then, we use $\bar{\sigma}\left(\bar{\lambda}_{\parallel}, \bar{\lambda}_{\perp}, \mu\right)$ and $\bar{\bar{\sigma}}\left(\bar{\lambda}_{\parallel}, \bar{\lambda}_{\perp}, \mu\right)$ to express the coefficients of $\bar{C}^{-1} \otimes \bar{C}^{-1}$ and $\bar{C}^{-1} \boxtimes \bar{C}^{-1}$ in Eq. (B.1), where

$$\begin{aligned}\bar{\sigma}\left(\bar{\lambda}_{\parallel}, \bar{\lambda}_{\perp}, \mu\right) = {} & \left((\det \bar{C})^{\frac{1}{2}}W'_{mix}\left((\det C)^{\frac{1}{2}}\right) - \frac{\mu}{\Omega}\right) \\ & + (\det \bar{C})^{\frac{1}{2}}W''_{mix}\left((\det \bar{C})^{\frac{1}{2}}\right)\end{aligned} \tag{B.6}$$

and

$$\bar{\bar{\sigma}}\left(\bar{\lambda}_{\parallel}, \bar{\lambda}_{\perp}, \mu\right) = -2(\det \bar{C})^{\frac{1}{2}}\left(W'_{mix}(\det \bar{C})^{\frac{1}{2}} - \frac{\mu}{\Omega}\right) \tag{B.7}$$

Finally, we substitute Eqs. (B.4), (B.5), (B.6), and (B.7) in Eq. (B.1), and we write the elastic moduli $\mathbb{C}$ in a more compact form using δ_1, δ_2, δ_3, δ_5, and δ_6 as coefficients of A and P. More explicitly,

$$\begin{aligned}\mathbb{C} = {} & \delta_1 A \otimes A + \delta_2(A \otimes P + P \otimes A) + \delta_3 P \otimes P + \delta_4 A \boxtimes A \\ & + \delta_5(A \boxtimes P + P \boxtimes A) + \delta_6 P \boxtimes P\end{aligned} \tag{B.8}$$

where

$$\delta_1 = 4\gamma G\frac{\lambda_{0\parallel}^4}{(\det C_0)^{\frac{1}{2}}} + \bar{\sigma}\left(\bar{\lambda}_{\parallel}, \bar{\lambda}_{\perp}, \mu\right)\bar{\lambda}_{\parallel}^{-4} \tag{B.9}$$

$$\delta_2 = \bar{\sigma}\left(\bar{\lambda}_{\parallel}, \bar{\lambda}_{\perp}, \mu\right)\bar{\lambda}_{\parallel}^{-2}\bar{\lambda}_{\perp}^{-2} \tag{B.10}$$

$$\delta_3 = \bar{\sigma}\left(\bar{\lambda}_{\parallel}, \bar{\lambda}_{\perp}, \mu\right)\bar{\lambda}_{\perp}^{-4} \tag{B.11}$$

$$\delta_4 = \bar{\bar{\sigma}}\left(\bar{\lambda}_{\parallel}, \bar{\lambda}_{\perp}, \mu\right)\bar{\lambda}_{\parallel}^{-4} \tag{B.12}$$

$$\delta_5 = \bar{\bar{\sigma}}\left(\bar{\lambda}_{\parallel}, \bar{\lambda}_{\perp}, \mu\right)\bar{\lambda}_{\parallel}^{-2}\bar{\lambda}_{\perp}^{-2} \tag{B.13}$$

$$\delta_6 = \bar{\bar{\sigma}}\left(\bar{\lambda}_{\parallel}, \bar{\lambda}_{\perp}, \mu\right)\bar{\lambda}_{\perp}^{-4} \tag{B.14}$$

Using Voigt notation, the fourth-order tensor becomes second order tensor; we can express the five independent components of the stiffness

tensor $\mathbb{C}$ as a second-order tensor utilizing the variables in Eq. (B.8) as follows:

$$\mathbb{C} = \begin{bmatrix} \delta_1+\delta_4 & \delta_2 & \delta_2 & 0 & 0 & 0 \\ \delta_2 & \delta_3+\delta_6 & \delta_3 & 0 & 0 & 0 \\ \delta_2 & \delta_3 & \delta_3+\delta_6 & 0 & 0 & 0 \\ 0 & 0 & 0 & \delta_6/2 & 0 & 0 \\ 0 & 0 & 0 & 0 & \delta_5/2 & 0 \\ 0 & 0 & 0 & 0 & 0 & \delta_5/2 \end{bmatrix} \tag{B.15}$$

Matrix (B.15) gives the components of $\mathbb{C}$ in a local basis with one of the axes parallel to the fiber a. To use it in our equilibrium equation it is necessary to transform the components to the lab frame. The change of basis formula for the elasticity tensor can be expressed in matrix form as:

$$[\mathbb{C}]_{e_1e_2e_3} = [K][\mathbb{C}]_{e_1'e_2'e_3'}[K]^{\mathrm{T}} \tag{B.16}$$

where K is the rotation matrix that accomplishes the basis change.

For the particular case of rotation through an angle θ – positive in a counter-clockwise sense – about the e_3 axes, the rotation matrix K reduces to:

$$[\mathrm{K}] = \begin{bmatrix} c^2 & s^2 & 0 & 0 & 0 & 2cs \\ s^2 & c^2 & 0 & 0 & 0 & -2cs \\ 0 & 0 & 1 & 0 & 0 & 0 \\ 0 & 0 & 0 & c & s & 0 \\ 0 & 0 & 0 & -s & c & 0 \\ -cs & cs & 0 & 0 & 0 & c^2-s^2 \end{bmatrix} \tag{B.17}$$

where $c = \cos\theta$, $s = \sin\theta$. The inverse matrix K^{-1} can be obtained simply by changing the sign of the angle θ.

Using Eqs. (B.15), (B.16), and (B.17), we could write the nonzero elements of the rotation matrix as follows

$$K_{11} = \sin^2\theta\left(\left(\delta_6+\delta_3\right)\sin^2\theta + \cos^2\theta\delta_2\right) + \cos^2\theta\left(\delta_2 \times \sin^2\theta + \cos^2\theta\left(\delta_4+\delta_1\right)\right) + 4\delta_5\sin^2\theta \tag{B.18}$$

$$K_{12} = \cos^2\theta\left(\left(\delta_4+\delta_1\right)\sin^2\theta + \delta_2\cos^2\theta\right) + \sin^2\theta\left(\delta_2\sin^2\theta + \cos^2\theta\left(\delta_6+\delta_3\right)\right) - 4\delta_5\cos^2\theta\sin^2\theta \tag{B.19}$$

$$K_{13} = \delta_3\sin^2\theta + \delta_2\cos^2\theta \tag{B.20}$$

$$K_{14} = 0 \qquad K_{15} = 0 \tag{B.21}$$

$$K_{16} = 2\delta_5\cos\theta\sin\theta\left(\cos^2\theta - \sin^2\theta\right) + \sin^2\theta\sin\theta\left(\cos\theta\sin\theta\left(\delta_6+\delta_3\right) - \delta_2\cos\theta\sin\theta\right) + \cos^2\theta\left(\delta_2\cos\theta\sin\theta - \cos\theta\sin\theta\left(\delta_4+\delta_1\right)\right) \tag{B.22}$$

$$K_{21} = K_{12} \tag{B.23}$$

$$K_{22} = \sin^2\theta\left(\left(\delta_4+\delta_1\right)\sin^2\theta + \delta_2\cos^2\theta\right) + \cos^2\theta\left(\delta_2\sin^2\theta + \cos^2\theta\left(\delta_6+\delta_3\right)\right) + 4\delta_5\cos^2\theta\sin^2\theta \tag{B.24}$$

$$K_{23} = \delta_2\sin^2\theta + \delta_3\cos^2\theta \tag{B.25}$$

$$K_{24} = 0 \qquad K_{25} = 0 \tag{B.26}$$

$$K_{26} = -2\delta_5\cos\theta\sin\theta\left(\cos^2\theta - \sin^2\theta\right) + \cos^2\theta\left(\cos\theta\sin\theta\left(\delta_6+\delta_3\right) - \delta_2\cos\theta\sin\theta\right) + \sin^2\theta\left(\delta_2\cos\theta\sin\theta - \cos\theta\sin\theta\left(\delta_4+\delta_1\right)\right) \tag{B.27}$$

$$K_{33} = \delta_3 + \delta_6 \tag{B.28}$$

$$K_{34} = 0 \qquad K_{35} = 0 \tag{B.29}$$

$$K_{36} = \delta_3\cos\theta\sin\theta - \delta_2\cos\theta\sin\theta \tag{B.30}$$

$$K_{45} = \delta_5\sin^2\theta + \delta_6\cos^2\theta \tag{B.31}$$

$$K_{46} = 0 \tag{B.32}$$

$$K_{55} = \delta_6\sin^2\theta + \delta_5\cos^2\theta \tag{B.33}$$

$$K_{56} = 0 \tag{B.34}$$

$$K_{66} = \delta_5\left(\cos^2\theta - \sin^2\theta\right)^2 + \cos\theta\sin\theta\left(\cos\theta\left(\delta_6+\delta_3\right) - \delta_2\cos\theta\sin\theta\right) - \cos\theta\sin\theta\left(\delta_2\cos\theta\sin\theta - \cos\theta\sin\theta\left(\delta_4+\delta_1\right)\right) \tag{B.35}$$

References

[1] G. Arranz, M. Moriche, M. Uhlmann, O. Flores, M. García-Villalba, Kinematics and dynamics of the auto-rotation of a model winged seed, Bioinspiration Biomim. 13 (3) (2018) 036011.

[2] C. Cummins, M. Seale, A. Macente, D. Certini, E. Mastropaolo, I.M. Viola, N. Nakayama, A separated vortex ring underlies the flight of the dandelion, Nature 562 (7727) (2018) 414–418.

[3] E. Reyssat, L. Mahadevan, Hygromorphs: from pine cones to biomimetic bilayers, J. R. Soc. Interface 6 (39) (2009) 951–957.

[4] S. Armon, E. Efrati, R. Kupferman, E. Sharon, Geometry and mechanics in the opening of chiral seed pods, Science 333 (6050) (2011) 1726–1730.

[5] H. Hofhuis, D. Moulton, T. Lessinnes, A.-L. Routier-Kierzkowska, R.J. Bomphrey, G. Mosca, H. Reinhardt, P. Sarchet, X. Gan, M. Tsiantis, et al., Morphomechanical innovation drives explosive seed dispersal, Cell 166 (1) (2016) 222–233.

[6] N.E. Stamp, Self-burial behaviour of Erodium cicutarium seeds, J. Ecol. (1984) 611–620.

[7] D. Evangelista, S. Hotton, J. Dumais, The mechanics of explosive dispersal and self-burial in the seeds of the filaree, Erodium cicutarium (Geraniaceae), J. Exp. Biol. 214 (4) (2011) 521–529.

[8] B. Mazzolai, T. Kraus, N. Pirrone, L. Kooistra, A. De Simone, A. Cottin, L. Margheri, Towards new frontiers for distributed environmental monitoring based on an ecosystem of plant seed-like soft robots, in: Proceedings of the Conference on Information Technology for Social Good, 2021, pp. 221–224.

[9] B. Mazzolai, S. Mariani, M. Ronzan, L. Cecchini, I. Fiorello, K. Cikalleshi, L. Margheri, Morphological computation in plant seeds for a new generation of self-burial and flying soft robots, Front. Robot. AI 8 (2021) 797556.

[10] S. Timoshenko, Analysis of bi-metal thermostats, Josa 11 (3) (1925) 233–255.

[11] Y. Klein, E. Efrati, E. Sharon, Shaping of elastic sheets by prescription of non-Euclidean metrics, Science 315 (5815) (2007) 1116–1120.

[12] J. Kim, J.A. Hanna, M. Byun, C.D. Santangelo, R.C. Hayward, Designing responsive buckled surfaces by halftone gel lithography, Science 335 (6073) (2012) 1201–1205.

[13] A.S. Kuenstler, Y. Chen, P. Bui, H. Kim, A. DeSimone, L. Jin, R.C. Hayward, Blueprinting photothermal shape-morphing of liquid crystal elastomers, Adv. Mater. 32 (17) (2020) 2000609.

[14] S. Abdelmohsen, S. Adriaenssens, R. El-Dabaa, S. Gabriele, L. Olivieri, L. Teresi, A multi-physics approach for modeling hygroscopic behavior in wood low-tech architectural adaptive systems, Comput. Aided Des. 106 (2019) 43–53.

[15] P. Nardinocchi, M. Pezzulla, L. Teresi, Anisotropic swelling of thin gel sheets, Soft Matter 11 (8) (2015) 1492–1499.

[16] Y. Liu, H. Zhang, J. Wang, Y. Zheng, Anisotropic swelling in fiber-reinforced hydrogels: An incremental finite element method and its applications in design of bilayer structures, Int. J. Appl. Mech. 8 (07) (2016) 1640003.

[17] P.J. Flory, J. Rehner Jr., Statistical mechanics of cross-linked polymer networks I. Rubberlike elasticity, J. Chem. Phys. 11 (11) (1943) 512–520.

[18] J. Zhang, X. Zhao, Z. Suo, H. Jiang, A finite element method for transient analysis of concurrent large deformation and mass transport in gels, J. Appl. Phys. 105 (9) (2009) 093522.

[19] P. Nardinocchi, M. Pezzulla, L. Teresi, Steady and transient analysis of anisotropic swelling in fibered gels, J. Appl. Phys. 118 (24) (2015) 244904.

[20] J. Merodio, R. Ogden, Mechanical response of fiber-reinforced incompressible non-linearly elastic solids, Int. J. Non-Linear Mech. 40 (2–3) (2005) 213–227.

[21] A.J. Spencer, Continuum Theory of the Mechanics of Fibre-Reinforced Composites, Springer, 1985.

[22] G.A. Holzapfel, Nonlinear Solid Mechanics: A Continuum Approach for Engineering Science, Kluwer Academic Publishers, Dordrecht, 2002.

[23] F. Horkay, G.B. McKenna, Polymer networks and gels, in: Physical Properties of Polymers Handbook, Springer, 2007, pp. 497–523.

[24] A. Lucantonio, P. Nardinocchi, L. Teresi, Transient analysis of swelling-induced large deformations in polymer gels, J. Mech. Phys. Solids 61 (1) (2013) 205–218.
[25] Y. Abraham, R. Elbaum, Hygroscopic movements in Geraniaceae: the structural variations that are responsible for coiling or bending, New Phytol. 199 (2) (2013) 584–594.
[26] L. Vannozzi, A. Lucantonio, A. Castillo, A. De Simone, L. Ricotti, Modeling self-rollable elastomeric films for building bioinspired hierarchical 3D structures, Int. J. Mol. Sci. 23 (15) (2022) 8467.
[27] D. Lunni, M. Cianchetti, C. Filippeschi, E. Sinibaldi, B. Mazzolai, Plant-inspired soft bistable structures based on hygroscopic electrospun nanofibers, Adv. Mater. Interfaces 7 (4) (2020) 1901310.
[28] C.P. Callaway, K. Hendrickson, N. Bond, S.M. Lee, P. Sood, S.S. Jang, Molecular modeling approach to determine the flory-huggins interaction parameter for polymer miscibility analysis, ChemPhysChem 19 (13) (2018) 1655–1664.